Clay Minerals (2020), **55**, 320–328
doi:10.1180/clm.2021.1

CAMBRIDGE UNIVERSITY PRESS

Article

Hydrothermal solidification of sepiolite into a cemented sepiolite aggregate for humidity regulation and formaldehyde removal

Pengcheng Qiu, Li Guo, Yujie Qi, Mingzhao Cheng and Zhenzi Jing*
Tongji University, School of Materials Science and Engineering, Shanghai, 201804, China

Abstract

Sepiolite powder was hydrothermally solidified into a cemented, designed to function both in humidity regulation and volatile organic compound (VOC) removal. The solidification process mimicked the cementation of sedimentary rocks. The formation of the calcium aluminium silicate hydrate (C-A-S-H) or Al-tobermorite enhanced the strength (maximum flexural strength >17 MPa) and improved the porosity of the solidified materials. Due to the low temperature of hydrothermal solidification (≤473.15 K), most sepiolite remained in the matrix of the solidified specimens. The cemented sepiolite aggregate shows outstanding humidity-regulating performance (moisture adsorption of 430 g m^{-2}), and the synergistic effects of the residual sepiolite and neoformed Al-tobermorite exerted a positive influence on the humidity regulation performance of the material. Similarly to the behaviour of sepiolite, the solidified material also displayed good formaldehyde-removal capacity (60–68%). The pore dimensions controlled the humidity regulation and formaldehyde removal. The humidity regulation depends on the mesopores, which originate mainly from both the original sepiolite and the neoformed C-A-S-H phases and Al-tobermorite, while the formaldehyde removal depends on the micropores from the original sepiolite in the matrix. As such, the cemented sepiolite aggregate might be hydrothermally synthesized and might be used to improve the comfort and safety of indoor environments for human beings.

Keywords: Al-tobermorite, C-A-S-H, cemented sepiolite aggregate, humidity self-regulation, hydrothermal solidification, VOC removal

(Received 4 July 2020; revised 27 December 2020; Accepted Manuscript online: 8 January 2021; Associate Editor: Huaming Yang)

Sepiolite ($Si_{12}Mg_8O_{30}(OH)_4(H_2O)_4{\cdot}8H_2O$), a natural sheet silicate with large specific surface area and abundant pores (Inagaki *et al.*, 1990), has been used widely as an adsorbent for organic compounds such as phenanthrene (Gonzalez-Santamaria *et al.*, 2017) and volatile organic compounds (VOCs; Kai *et al.*, 2011; Shen, 2019), and as a humidity controller to regulate indoor humidity (Gonzalez *et al.*, 2001; Yamaguchi, 2012; Cho *et al.*, 2020). Due to its excellent adsorption properties, sepiolite was used as the filter tips of cigarettes in the mid-eighteenth century (Zhang, 2000) and more recently has been used in the famous Turkish tobacco pipes, where it can be used to reduce tar and nicotine levels. Sepiolite powders have also been used as coatings and wallpapers for regulating humidity and thus improving indoor air quality since the 1970s (Wu *et al.*, 2014). However, the natural sepiolite in China, referred to as sepiolite clay, is rich in impurities and is utilized only in the form of powders with low mechanical strength. Therefore, natural sepiolite cannot be used directly as a building material and its further application is greatly limited. The best way to tackle this problem is to convert the sepiolite clay into a cemented sepiolite aggregate for further use.

To obtain mechanically strong building materials, the traditional sintering method (≥1173.15 K) is used widely. The inherent properties and performance of the original materials might be preserved when the processing temperature does not exceed 773.15 K (Ishida, 2002). Therefore, transformation of natural sepiolite into a tough matrix that still retains the inherent microstructure and performance of the original sepiolite is a critical step.

By mimicking the lithification processes and using the hardening mechanisms of cement and concrete, a cemented sepiolite aggregate was obtained from natural sepiolite clay under hydrothermal treatment with calcium aluminium silicate hydrate (C-A-S-H) or Al-tobermorite formation, and because of the low temperature (≤473.15 K) of hydrothermal solidification, the microstructure (porosity) of raw sepiolite might be preserved in the matrix of the sepiolite specimens (Sarıkaya *et al.*, 2020). The hydrothermal technology has been applied widely not only in inorganic material synthesis, but also in organic material compositions (Lyu *et al.*, 2014; He *et al.*, 2019).

Suitable relative humidity (RH) not only creates a comfortable environment, but may also restrict bacteria and virus reproduction. A RH ranging from 40 to 70% is considered to be the most comfortable for human beings (Arundel *et al.*, 1986). The VOCs mainly emanating from indoor materials such as coatings, adhesive agents, *etc.* (Shang *et al.*, 2002), may cause serious harm to human health, even at very low concentrations (Xu *et al.*, 2018), and therefore the removal of indoor VOCs is extremely important.

The adsorption behaviour of moisture and VOCs may be described using various isotherm models. According to the classification of the International Union of Pure and Applied

*Email: zzjing@tongji.edu.cn
Cite this article: Qiu P, Guo L, Qi Y, Cheng M, Jing Z (2020). Hydrothermal solidification of sepiolite into a cemented sepiolite aggregate for humidity regulation and formaldehyde removal. *Clay Minerals* **55**, 320–328. https://doi.org/10.1180/clm.2021.1

Chemistry (IUPAC), the moisture adsorption isotherm belongs to type IV, which indicates the presence of mesopores exhibiting adsorption hysteresis characteristics. Our previous work showed that a pore size from 4.2 to 7.1 nm, such as those found in mesoporous materials, leads to effective moisture adsorption/desorption performance for humidity regulation (Lan *et al.*, 2017). On the other hand, the isotherm of formaldehyde adsorption is of type I (Song *et al.*, 2007), which exhibits mainly microporous adsorption characteristics. The diameter of formaldehyde molecules is ~0.45–0.75 nm, and based on the Horvath–Kawazoe (HK) method (Chen *et al.*, 1996), the effective pore size for adsorption should be as small as one or two times that of the adsorbate. Therefore, materials with micropores should have a good VOC (formaldehyde) removal efficiency (Chen *et al.*, 1996). As sepiolite is rich in micropores and mesopores (Sun *et al.*, 1995), aggregates of this mineral with both types of porosity would be useful as functional materials that have humidity-regulating and VOC-adsorbing capacities.

To the best of our knowledge, the hydrothermal solidification of sepiolite clay into a cemented sepiolite aggregate for humidity regulation and VOC (formaldehyde) adsorption has not been reported before. The present work aims to: (1) transform the sepiolite into a tough sepiolite-based material (cemented sepiolite aggregate) and determine its hardening mechanism; (2) study the humidity-regulating property of the cemented sepiolite aggregate and improve this humidity-regulating performance; and (3) study the VOC (formaldehyde) adsorption and its mechanism. The results are expected to provide practical information on a cemented sepiolite aggregate that might be used directly indoors for both humidity regulation and VOC adsorption.

Experimental

Sepiolite raw material

The sepiolite used in this study was obtained from HongYan Sepiolite Corporation, Ltd, in Hunan Province, China. Reagent-grade calcium hydroxide ($Ca(OH)_2$), obtained from Sinopharm Chemical Reagent (Shanghai, China), was used as an additive. The sepiolite was ground in a ball mill to pass through a 100-mesh sieve. The particle-size distribution curve of the sepiolite is shown in Fig. 1. The main chemical components of the sepiolite (Table 1) are SiO_2 (58.7 mass%) and Al_2O_3 (11.9 mass%). CaO (1.73 mass%) is a minor component. The semi-quantitative analysis based on the X-ray diffraction (XRD) traces (Fig. 2) shows that the main phases in the original material are sepiolite (73.1%), quartz (13.7%) and talc (10.8%). The Fourier-transform infrared (FTIR) spectrum of the sepiolite is shown in Fig. 2. The bands at 3623, 3557 and 3425 cm^{-1} correspond to Al–OH stretching vibrations (Ahlrichs *et al.*, 1975) and the bands centred at 1664 and 691 cm^{-1} are due to stretching vibrations of Mg–OH groups. The stretching bands at 1031 and 471 cm^{-1} belong to Si–O–Si groups of the tetrahedral sheet, while the stretching bands at 798 and 780 cm^{-1} belong to Si–O bonds (Fig. 2) (Liang *et al.*, 2011; Ozcan *et al.*, 2012).

Hydrothermal solidification

The dried sepiolite powder (353.15 K, 24 h) mixed at various ratios (0–50 mass%) with $Ca(OH)_2$ were used as starting materials. The starting materials were mixed manually with 30 mass% distilled water using a pestle and mortar, and then the mixtures were compacted by uniaxial pressure of 30 MPa in a rectangular mould (40 mm × 15 mm × 5 mm). The green specimens were treated in a Teflon-lined stainless-steel autoclave under saturated steam pressure at 373.15–513.15 K for up to 12 h, and after hydrothermal processing the specimens were dried in air at 353.15 K for 24 h before testing.

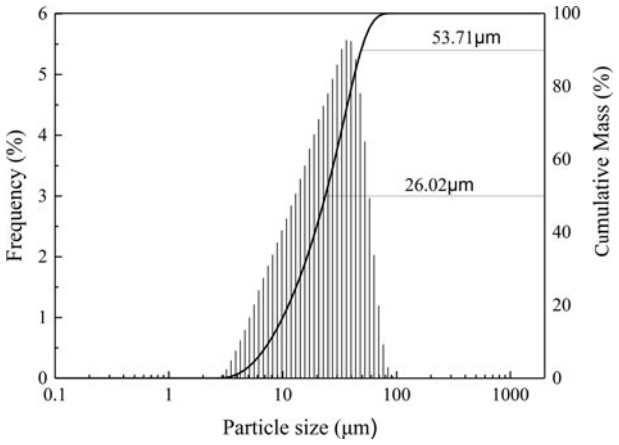

Fig. 1. Particle-size distribution of raw sepiolite.

Table 1. Chemical composition of raw sepiolite (mass%).

Component	Na_2O	MgO	Al_2O_3	SiO_2	P_2O_5	K_2O	CaO	Fe_2O_3	LOI
Content	0.79	12.3	11.9	58.7	8.25	0.81	1.73	3.48	2.04

LOI = loss on ignition.

Characterization

The chemical analysis (major elements) of the raw material was performed using an X-ray fluorescence (XRF) spectrometer (Rigaku RIX 3100, Japan). The particle size of the raw material was investigated *via* laser diffraction analysis (LPSA, Malvern 2000) using distilled water to prepare the suspension. The hydrothermally synthesized specimens (40 mm × 15 mm × 5 mm) were used to measure the three-point flexural strength, employing the Japanese industrial standard (JIS R1601) at a loading rate of 0.5 mm min^{-1} using a universal testing machine (XO-106A, Xie Qiang Instrument Technology). All flexural strength values reported here are averages of three measurements obtained for three different samples.

The crushed specimens were then investigated using several analytical techniques. The crystalline phases were determined *via* XRD (Bruker D8 Advance Powder Diffractometer) at 40 kV and 60 mA using Cu-*Kα* radiation (λ = 1.54 Å, scanning range 5–60°2θ, scanning speed 5° min^{-1}). *Jade 6* software with reference data (PDF 2004 database) was utilized to identify the mineral phases and to perform the semi-quantitative analysis. The FTIR spectra of the materials were obtained by FTIR spectrometry (EQUINOXSS FTIR spectrometer) using the KBr pellet technique. The fracture surface morphology was examined using an environmental scanning electron microscope (ESEM; Quanta 200 FEG ESEM) on samples that had previously been gold-sputtered (10 nm thick). The specific surface area and total pore volume were determined using nitrogen gas sorption analysis at

https://doi.org/10.1180/clm.2021.1 Published online by Cambridge University Press

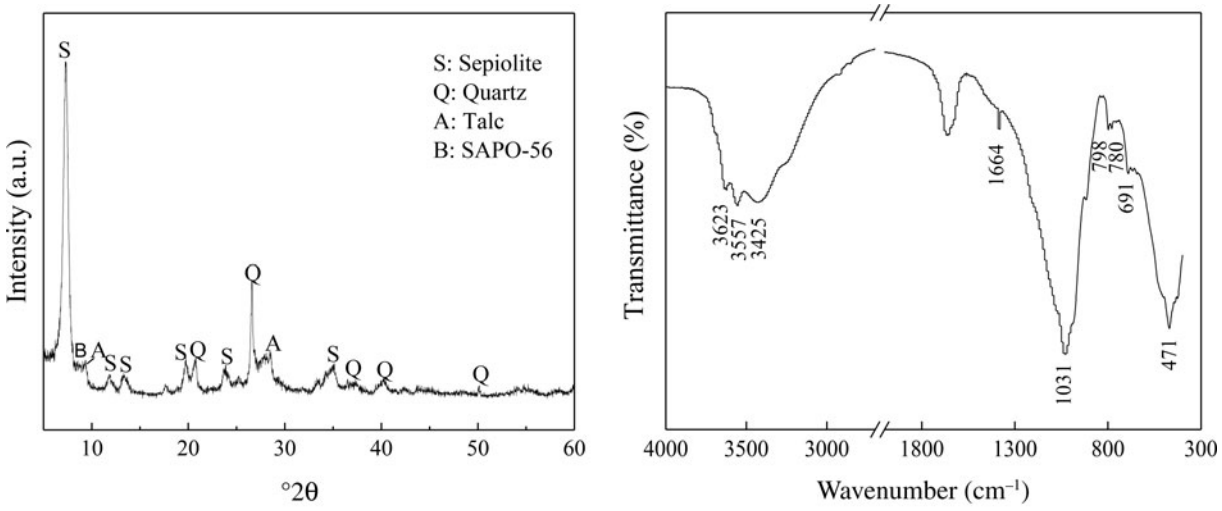

Fig. 2. XRD trace (left) and FTIR spectrum (right) of raw sepiolite.

77.15 K (Autosorb-1 Quantachrome Instruments, Boynton Beach, FL, USA) based on the Brunauer–Emmett–Teller (BET) equation.

The humidity-regulating apparatus (Fig. 3) and measurements were developed according to Japanese industrial standards (JIS A 1470-1, 2:2008). The surfaces of the specimens, except for their top surface, were covered with aluminium tape to ensure that the adsorbed/desorbed water vapour would only migrate through the top surface. The specimens were placed in an airtight box with a RH of 75% for 24 h, and then at a RH of 33% for another 24 h. The RHs of 75% and 33% in the airtight box were controlled by $MgCl_2{\cdot}6H_2O$ and NaCl saturated salt solutions, respectively. During this process, the mass change of the specimens due to moisture adsorption/desorption was measured every 10 min.

The apparatus for investigating the formaldehyde adsorption was built based on Chinese industry standards (GB/T35243-2017). The specimens were placed in the sealed apparatus, then a constant formaldehyde concentration of 1 mg m^{-3} was set up in the sealed apparatus, and the formaldehyde concentration variation due to adsorption of the sepiolite specimen was measured every 30 min with a formaldehyde testing instrument (PPM-400ST) at a controlled temperature of 296.15 K. The adsorption ratio, calculated using the equation $100(C_0 - C_t)/C_0\%$, where C_0 is the initial formaldehyde concentration and C_t is the formaldehyde concentration at time t, was used to evaluate the formaldehyde adsorption.

Results and discussion

Effect of Ca(OH)$_2$ content

Based on the hardening mechanism of cement and concrete and because the sepiolitic raw material is rich in SiO_2 and poor in CaO (Table 1), $Ca(OH)_2$ should be introduced to form C-A-S-H or Al-tobermorite to enhance the strength of specimens (Sun *et al.*, 2015; Miao *et al.*, 2018).

The flexural strengths of the specimens mixed with various $Ca(OH)_2$ contents and cured at 473.15 K for 12 h are shown in Fig. 4. The flexural strength of the raw sepiolite (0 mass% $Ca(OH)_2$) is rather low (2.4 MPa); with increasing additions of $Ca(OH)_2$, the flexural strength of the specimens increases significantly. At 30 mass% $Ca(OH)_2$, the flexural strength is maximized (11 MPa), which is almost four times greater than that of the sepiolite specimen at 0 mass% $Ca(OH)_2$. This strength decreases with greater additions of $Ca(OH)_2$.

The phase evolution within the matrix with increasing $Ca(OH)_2$ was investigated by XRD (Fig. 5). The semi-quantitative mineralogical composition of the samples is listed in Table 2. The original sample consists mainly of sepiolite with minor quartz and talc, which gradually decrease with increasing $Ca(OH)_2$ contents due to the reaction with $Ca(OH)_2$. Concurrently, the C-A-S-H phases appear at 10 mass% $Ca(OH)_2$ and Al-tobermorite begins to form after addition of 20 mass% $Ca(OH)_2$ addition. Al-tobermorite may partly form from C-A-S-H phases because Al is contained in the raw material (Schreiner *et al.*, 2020). Both C-A-S-H and Al-tobermorite are maximized when 30 mass% $Ca(OH)_2$ is added. However, with further addition of $Ca(OH)_2$, Al-tobermorite tends to disappear (Table 2). The excessive addition of $Ca(OH)_2$ forms a protective coating on the surface of anhydrous particles and thus may inhibit further hydration. The formation of Al-tobermorite and C-A-S-H phases might be related to the observed increase in flexural strength, in agreement with previous work (Zhang *et al.*, 2013). In addition, most sepiolite is still present in the matrix at 30 mass% $Ca(OH)_2$ (the maximum strength) (see the inset in Fig. 5 and Table 2).

The FTIR spectra of the specimens with various $Ca(OH)_2$ contents cured at 473.15 K for 12 h are shown in Fig. 6. With increasing $Ca(OH)_2$ content, the bands corresponding to the stretching vibrations of sepiolite (1028, 799, 780 and 692 cm^{-1}; Liang *et al.*, 2011) tend to weaken, and a new band appears at 970 cm^{-1}, which might be attributed to Al-tobermorite and C-A-S-H phases (Miao *et al.*, 2018). Therefore, in agreement with the XRD results, the addition of $Ca(OH)_2$ initially contributes to the transformation of sepiolite and the formation of Al-tobermorite and C-A-S-H phases, which results in increased strength. With further addition of $Ca(OH)_2$ (to 40 mass%), the band intensity at 970 cm^{-1} tends to decrease because excessive $Ca(OH)_2$ addition limits hydration, which is in agreement with the XRD results (Fig. 5). The migration of the Si–O band from 1028 to 970 cm^{-1} might be related to the decrease in the degree of polymerization of $[SiO_4]^{4-}$ units because the raw materials contain certain amounts of Al^{3+} (Table 1), and thus the Si^{4+} in the $[SiO_4]^{4-}$ tetrahedra may be partially replaced by Al^{3+} to form

https://doi.org/10.1180/clm.2021.1 Published online by Cambridge University Press

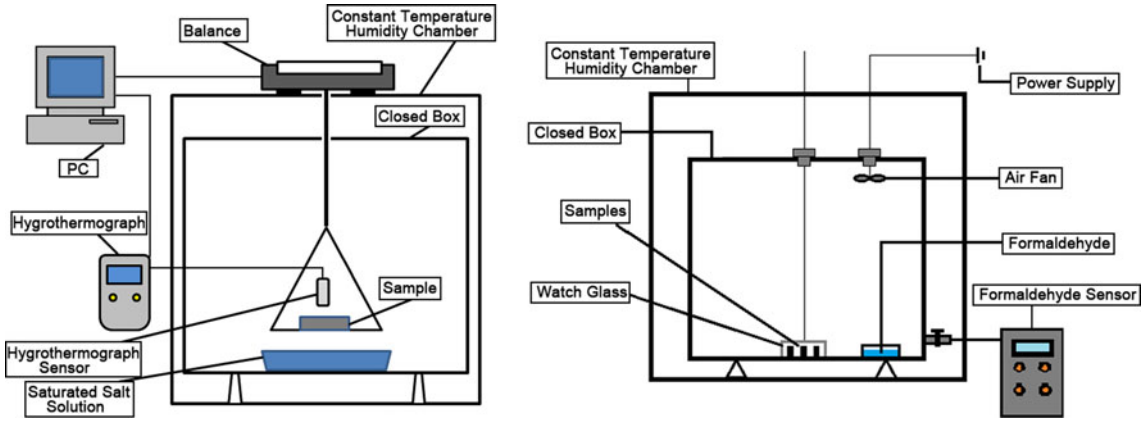

Fig. 3. Apparatus for measuring the humidity-regulating (left) and formaldehyde-adsorption (right) properties of the materials.

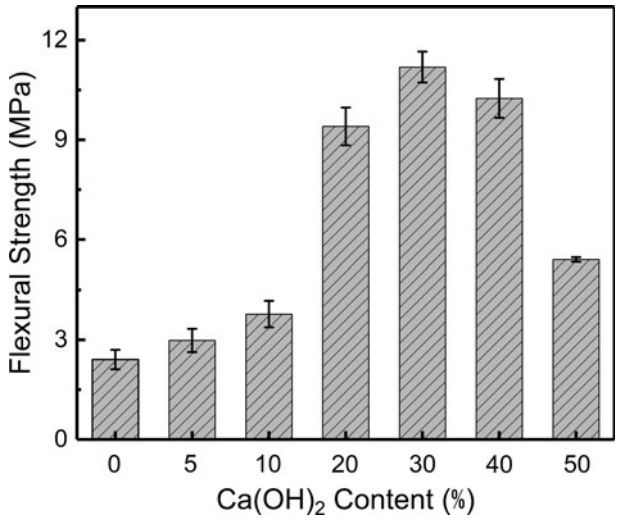

Fig. 4. Effects of $Ca(OH)_2$ content on the flexural strength of specimens cured at 473.15 K for 12 h.

alumina polyhedrons (*i.e.* Al-tobermorite and C-A-S-H phases; Li *et al.*, 2020). The band at 1028 cm^{-1} is still of high intensity, indicating that most sepiolite might survive after the hydrothermal reaction. Therefore, to synthesize the cemented sepiolite aggregate, the addition of 30 mass% $Ca(OH)_2$ was used throughout this study.

Effect of curing conditions

The effects of curing time and temperature on the flexural strength were investigated. The strength evolution of specimens cured at 473.15 K for various curing times and cured for 6 h at various temperatures are shown in Fig. 7. The flexural strength increases rapidly up to 3 h curing time, reaching a maximum strength (>17 MPa) at 6 h, which is three times greater than that without curing (0 h). For greater curing times, the flexural strength declines gradually. The flexural strength is also influenced by the curing temperature. It increases gradually to >17 MPa until 473.15 K, and then decreases to 13 MPa at 513.15 K.

The XRD traces of specimens cured at 473.15 K for various curing times and specimens cured for 6 h at various temperatures are shown in Fig. 8 and the semi-quantitative composition is listed in Table 3. Sepiolite, quartz, talc and portlandite continuously decrease while some C-A-S-H phases and Al-tobermorite appears, suggesting more sepiolitic raw material and $Ca(OH)_2$ transfer to C-A-S-H phases and Al-tobermorite for higher curing times or temperatures (Table 4). Comparison of these phase evolutions with the strength development shows that the C-A-S-H phases and Al-tobermorite formation enhance the strength. Al-tobermorite crystals will grow at longer curing times or higher curing temperatures, and the overgrowth of Al-tobermorite may loosen the matrix, thus exerting a minor influence on the strength. It should be noted that the sepiolite phase exists in all of the synthesized specimens (Table 4), while the Al-tobermorite formed at longer curing times and higher curing temperatures may lead to the formation of a tough matrix. As such, a cemented sepiolite aggregate material might be solidified hydrothermally with sepiolite clay powder.

The ESEM micrographs (Fig. 9) reveal the change in the phase morphology of the specimens cured at 473.15 K for 0 and 6 h. Before the hydrothermal treatment (0 h), a mass of fibrous sepiolite, rod-like talc and massive quartz can be observed clearly in the matrix. After 6 h of curing (Fig. 9b), some needle-like or tabular crystals of Al-tobermorite and flocculating C-A-S-H (Li *et al.*, 2020) form, filling the spaces between the sepiolite fibres, thus enhancing the flexural strength and forming a cemented sepiolite aggregate. In addition, some mesopores form on the surface of the Al-tobermorite crystals (Fig. 9c) and intercrystallite mesopores appear between crosslinked Al-tobermorite crystals (Fig. 9d). Therefore, the formation of Al-tobermorite may not only enhance strength, but also increase mesoporosity.

Adsorption performance and mechanism

The performance of the cemented sepiolite aggregate was tested for humidity-regulation and formaldehyde-adsorption properties in specimens with the addition of 30 mass% $Ca(OH)_2$ and cured at 473.15 K for 0, 6 and 12 h.

Humidity-regulating capacity

Figure 10 displays the moisture adsorption/desorption performance of the specimens when the RH of the environment changed from 75% to 33% at 298.15 K for various curing times. At 0 h curing time, the specimen exhibits good moisture adsorption performance (moisture adsorption of 230 g m^{-2}) due to the presence of the sepiolite in the matrix. After 6 h of curing time,

https://doi.org/10.1180/clm.2021.1 Published online by Cambridge University Press

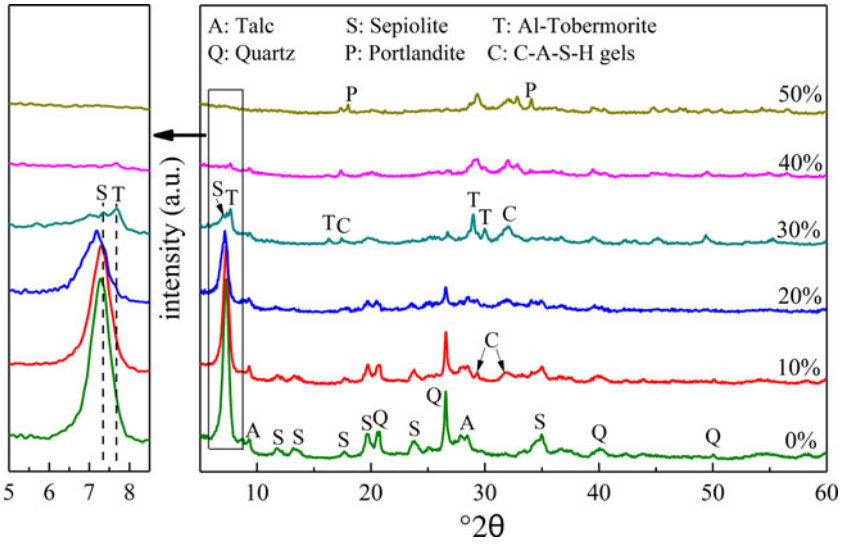

Fig. 5. XRD traces of samples containing various proportions of $Ca(OH)_2$ and cured at 473.15 K for 12 h.

Table 2. Semi-quantitative composition of samples containing various $Ca(OH)_2$ contents (%).

	Sepiolite	Quartz	Talc	C-A-S-H	Al-tobermorite	Portlandite
0%	72.0	13.8	14.2	–	–	–
10%	66.5	9.7	10.9	12.9	–	–
20%	40.1	4.9	9.2	38.9	6.9	–
30%	38.1	3.6	6.5	14.7	37.1	–
40%	5.2	6.2	15.4	45.5	17.9	9.8
50%	4.4	4.1	4.6	46.3	7.4	23.1

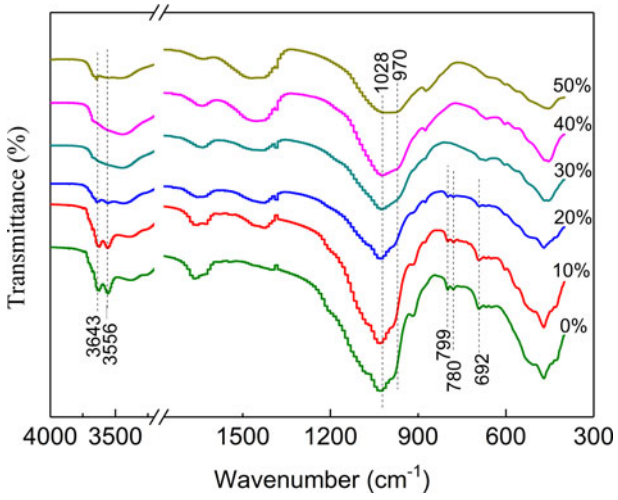

Fig. 6. FTIR spectra of samples containing various proportions of $Ca(OH)_2$ and cured at 473.15 K for 12 h.

maximum moisture adsorption occurred, exceeding 430 g m^{-2} – nearly twice that achieved without curing (0 h). This increase in moisture adsorption might be mainly due to the neoformed phases within the matrix, namely Al-tobermorite and C-A-S-H phases, and the mesopores formed on the surface and between the crystals of Al-tobermorite (Fig. 9). This suggests that the formed Al-tobermorite and C-A-S-H phases may not only enhance strength, but also improve the moisture adsorption/desorption (humidity-regulation) performance.

A detailed investigation of the microstructure (porosity) evolution of the specimens with various curing times was conducted to study the improvement in humidity regulation. The pore-size distributions of the specimens cured for 0, 6 and 12 h are shown in Fig. 11 and their specific surface areas and pore volumes are listed in Table 4.

The specific surface areas of specimens without curing (0 h) is only 62.50 m^2 g^{-1} and the total pore volume is 0.2168 cm^3 g^{-1}. After curing for 6 h, the specific surface area increases nearly two-fold (111.48 m^2 g^{-1}) and the pore volume also increases markedly. For specimens cured for 12 h, the specific surface area and pore volume decrease to 101.781 m^2 g^{-1} and 0.2800 cm^3 g^{-1}, respectively.

Before hydrothermal processing (0 h), the pore sizes range from 5 to 42 nm, corresponding to the spaces between sepiolite fibres (Fig. 11). After hydrothermal processing, the size of mesopores increases significantly. After curing for 6 h, more mesopores form, especially in the 4–9 nm range, which also results in the largest specific surface area (111.48 m^2 g^{-1}) and pore volume (0.3576 cm^3 g^{-1}; Table 5). A pore size of 4.2–7.1 nm might provide effective humidity regulation (Lan *et al.*, 2017) and might explain why curing for 6 h yields the best moisture adsorption/desorption (humidity-regulation) performance. As was mentioned above, after 6 h of curing, abundant sepiolite crystals remained in the matrix, and at the same time Al-tobermorite formed. The Al-tobermorite might enhance strength and may also markedly improve pore-size distribution, specific surface area and pore volume, thus significantly promoting humidity regulation.

The water-vapour adsorption/desorption isotherms of the solidified sediment specimens cured for various times are shown in Fig. 12. The water-vapour adsorption/desorption without hydrothermal processing is low, with few changes between 0.3 and 0.8 relative water-vapour pressure (30–80% RH). After curing for 6 h, the water-vapour adsorption/desorption capacity was greatly improved and the amount of the adsorbed/desorbed water increased from ~20 to 146 mg g^{-1}. The improvement in humidity regulation is probably due to the retained sepiolite and the formation of Al-tobermorite (Fig. 8 & Table 3), which in turn enhanced porosity (Figs 9 & 11). However, when the curing time extended to 12 h, the amount of adsorbed/desorbed water decreased to 117 mg g^{-1}, probably because of the

https://doi.org/10.1180/clm.2021.1 Published online by Cambridge University Press

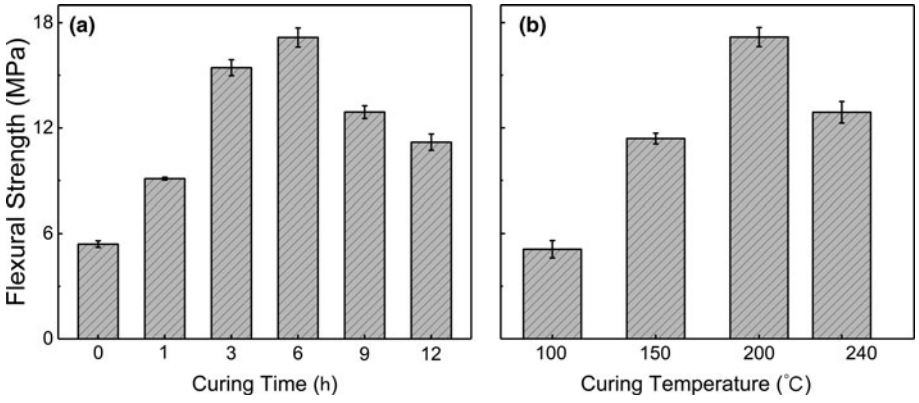

Fig. 7. Effects of (a) curing times and (b) temperatures on the flexural strength of specimens.

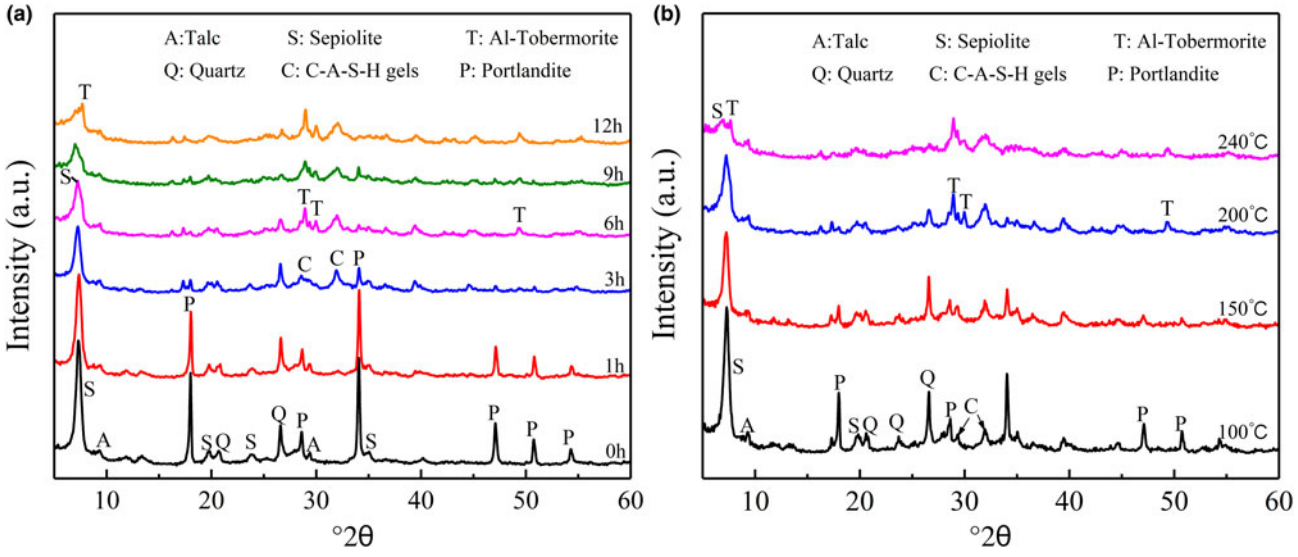

Fig. 8. XRD patterns of solidified specimens at (a) various curing times and (b) various temperatures.

Table 3. Semi-quantitative composition of solidified specimens cured at 473.15 K for various curing times and cured for 6 h at various temperatures.

	Sepiolite	Quartz	Talc	C-A-S-H	Al-tobermorite	Portlandite
0 h	53.8	8.3	6.5	–	–	31.4
1 h	49.8	6.8	5.7	9.3	–	28.4
3 h	31.0	5.7	9.9	41.5	4.2	7.8
6 h	30.2	2.3	8.0	30.7	24.1	4.8
9 h	34.1	5.7	14.4	12.6	30.3	3.5
12 h	38.1	3.6	6.5	14.7	37.1	–
373.15 K	35.9	5.1	2.6	42.5	0.5	13.5
423.15 K	33.6	7.7	7.4	33.2	9.8	8.3
473.15 K	30.2	2.3	8.0	30.7	24.1	4.8
513.15 K	30.9	2.8	11.2	18.5	34.6	2.8

disappearance of sepiolite (Fig. 6) and the overgrowth of Al-tobermorite crystals, which might reduce mesopores.

Formaldehyde-removal properties

Figure 13 shows the VOC (formaldehyde) adsorption ratio of specimens at various curing times. The greatest formaldehyde removal (70%) was observed in the sample without hydrothermal processing (0 h), followed by the sample cured for 6 h (68%), while the sample cured for 12 h adsorbed ~60% of the formaldehyde after 4 h. According to the peak intensity change with various curing times in the XRD traces (Fig. 8b), the formaldehyde removal seems to be related to the residual sepiolite content in the matrix (*i.e.* the more residual sepiolite, the greater the formaldehyde removal; Table 3). The formaldehyde removal seems not to depend on the mesopores because the specimens cured for 6 and 12 h have more mesopores than those without curing.

Table 4. Specific surface areas and pore volumes of specimens cured at 473.15 K for 0, 6 and 12 h.

Curing time (h)	Specific surface area ($m^2\ g^{-1}$)	Total pore volume ($cm^3\ g^{-1}$)
0	62.50	0.2168
6	111.48	0.3576
12	101.78	0.2800

As was mentioned before, the sepiolite itself is also rich in micropores, and an investigation into the change in the pore-size distribution of the specimens at various curing times (0 and 12 h) was conducted (Fig. 14). The hydrothermal processing does not affect the micropore size, which varies between 0.35 and 0.75 nm in the uncured and the cured samples, and this might be mainly

https://doi.org/10.1180/clm.2021.1 Published online by Cambridge University Press

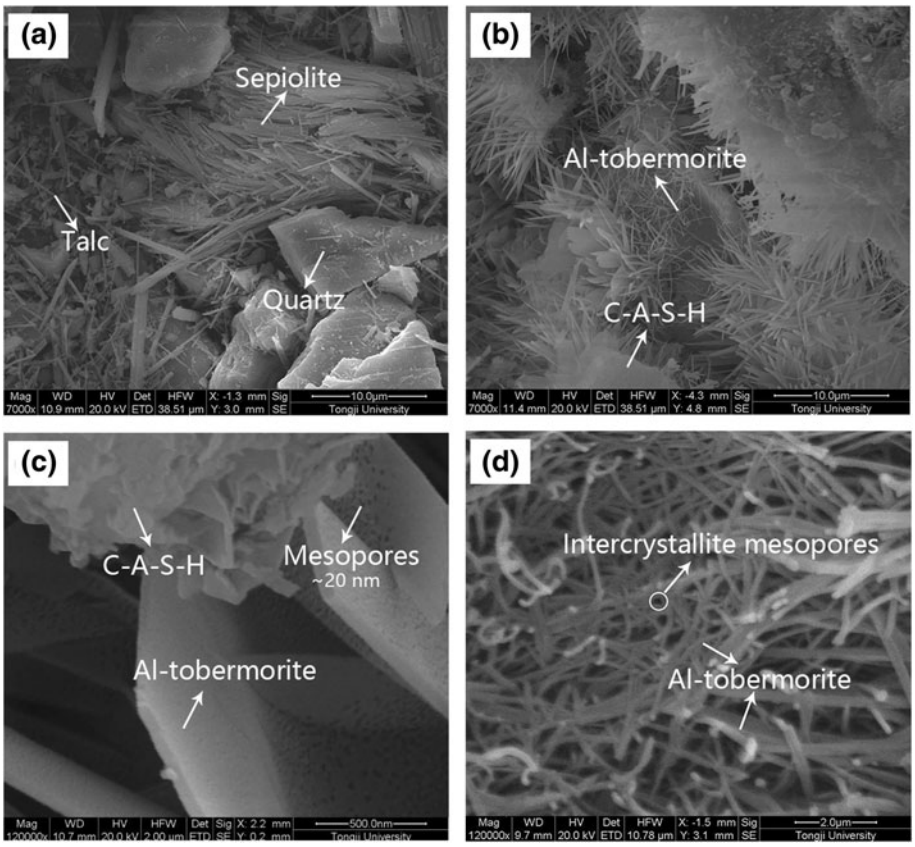

Fig. 9. ESEM images of specimens cured at 473.15 K for (a) 0 h and (b–d) 6 h.

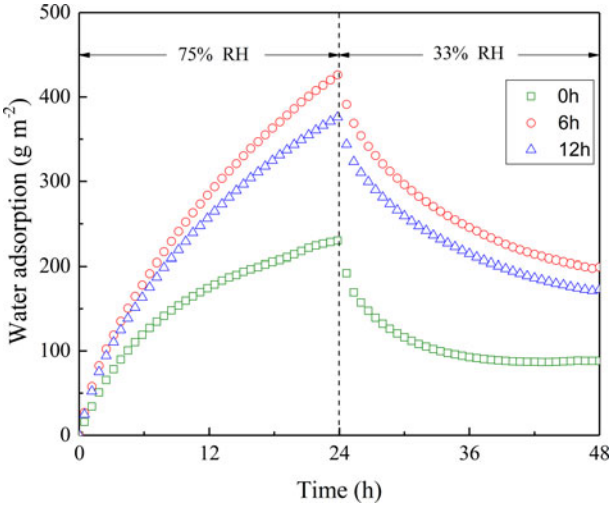

Fig. 10. Humidity-regulating properties of specimens cured at 473.15 K for various curing times.

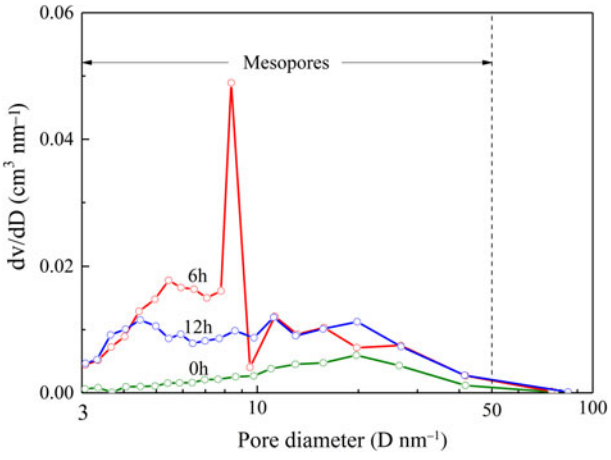

Fig. 11. Pore-size distributions of specimens cured for various curing times.

attributed to the microporous structure of sepiolite. Nevertheless, although after hydrothermal processing, the D(50) value of the specimens cured for 0 and 12 h is almost the same, there seem to be fewer micropores in the specimen cured for 12 h. This confirms the notion that the micropores probably originate from the sepiolite, not from the neoformed Al-tobermorite, which is also in accordance with the semi-quantitative XRD data (Table 3). With increasing curing time, the remaining sepiolite decreases due to its reaction to form Al-tobermorite (Fig. 8 & Table 3), which inevitably decreases the number of micropores within the matrix, thus resulting reduced formaldehyde removal.

Table 5. Constants and coefficients of determination of the Langmuir model.

Adsorbate	q_c	k	R^2
0	428.93	0.13	0.8848
6	13.85	1.18	0.9981

https://doi.org/10.1180/clm.2021.1 Published online by Cambridge University Press

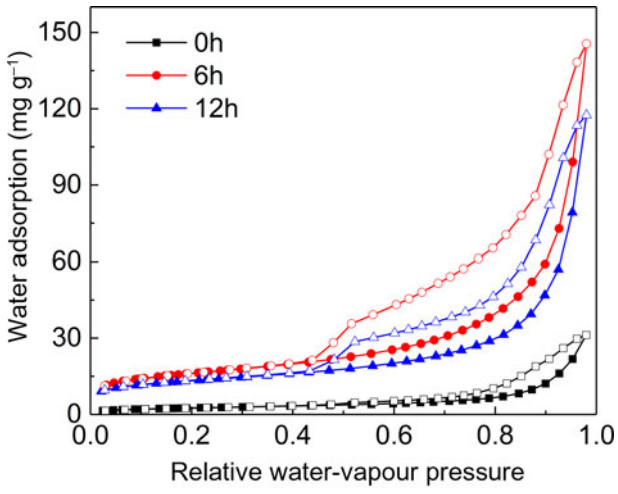

Fig. 12. Water-vapour isotherms at 25°C for the specimens cured for various curing times. Solid and open symbols represent adsorption and desorption isotherms, respectively.

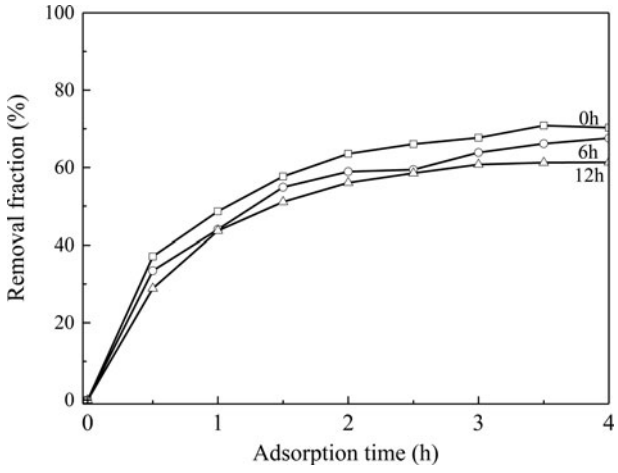

Fig. 13. Formaldehyde-adsorption capacity of specimens cured at 473.15 K for various curing times.

As discussed above, it seems that the formaldehyde adsorption depends mainly on the inherent micropores of sepiolite, while the neoformed Al-tobermorite seems to be less important in this study. The experimental data regarding the humidity regulation and formaldehyde adsorption of the specimens cured at 473.15 K for 6 h were used to fit the Langmuir isotherm models according to Eq. (1):

$$\log(q_c - q_e) = \log q_e - \frac{k}{2.303}t \quad (1)$$

where q_c and q_e (mg g^{-1}) are the uptakes of moisture or formaldehyde per unit mass of adsorbent at time t and saturation time and k is the Langmuir constant related to the rate of adsorption. The calculated constants are presented in Table 5.

The calculated Langmuir isotherm gives a good fit only for formaldehyde adsorption, with a goodness of fit value of R^2 >0.99 (Table 5). By contrast, the coefficient of determination for moisture adsorption according to the Langmuir model is low (R^2 = 0.88). This suggests that the formaldehyde adsorption isotherm belongs to type IV, and thus its adsorption depends mainly on the micropores in the matrix, which is in agreement with the results of this and previous work (Chen *et al.*, 1996). According to our previous work, a pore size of 4.2–7.1 nm in the materials led to effective moisture adsorption/desorption performance (Lan *et al.*, 2017), which might explain why the moisture adsorption data the had a poor fit with type I adsorption isotherm.

Conclusions

To extend the applications of sepiolite, hydrothermal synthesis of a cemented sepiolite aggregate for humidity regulation and formaldehyde adsorption was conducted, and the results are summarized as follows:

(1) The sepiolite was solidified into a cemented aggregate with maximum flexural strength of >17 MPa, in which most sepiolite still remained in the matrix due to the low-temperature hydrothermal synthesizing approach (≤473.15 K). The formation of C-A-S-H phases and Al-tobermorite enhanced

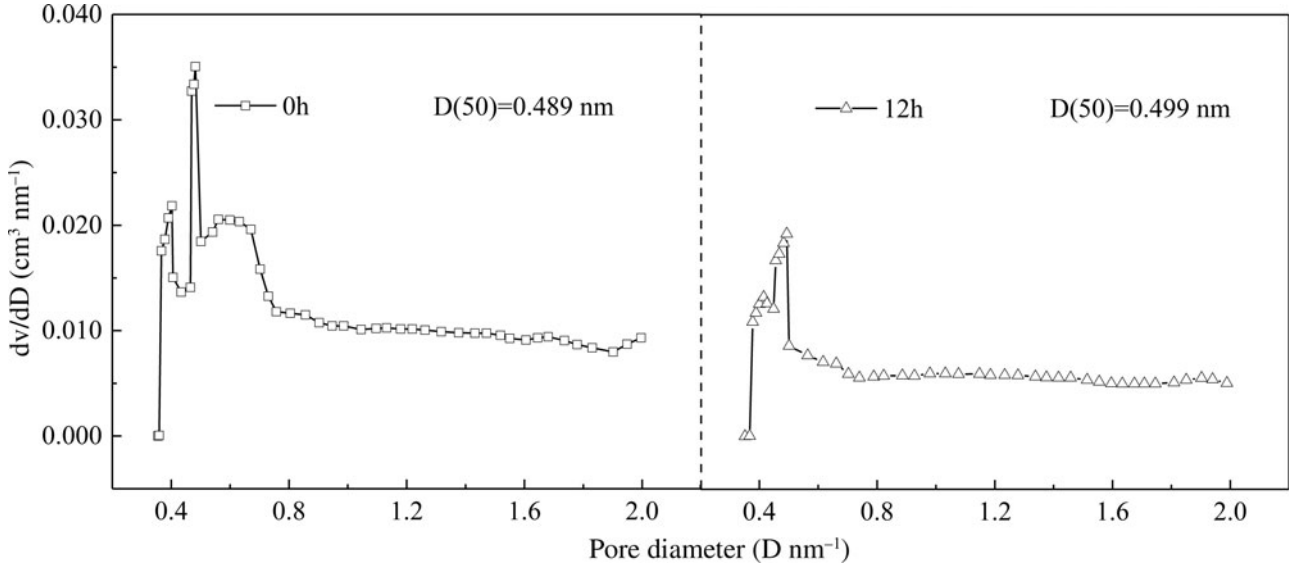

Fig. 14. Pore-size distributions of specimens cured for various curing times.

https://doi.org/10.1180/clm.2021.1 Published online by Cambridge University Press

the strength of the specimens, and $Ca(OH)_2$ addition, curing temperature and time influenced their formation.

(2) The porosity (pore-size distribution, specific surface area and pore volume) of the specimens is the key factor for humidity regulation. The mesopores from to the sepiolite and the C-A-S-H and Al-tobermorite phases formed increased the moisture adsorption/desorption performance significantly. The moisture adsorption of the specimen cured for 6 h exceeded 430 g m^{-2}, which is nearly twice that of the original sepiolite specimen without hydrothermal processing.

(3) Similarly to the original sepiolite, the produced material also displayed good formaldehyde removal (60–68%). However, by contrast to the humidity regulation, the micropores originating mainly from the remaining sepiolite in the matrix and not from the neoformed C-A-S-H phases and Al-tobermorite controlled formaldehyde removal.

Sepiolite can be converted hydrothermally into a cemented sepiolite aggregate with the capacity for humidity regulation and formaldehyde removal, and this aggregate might be used as a building material to provide comfortable and safe living conditions indoors.

Financial support. This work was supported by the National Natural Science Foundation of China (nos. 51872206, 51272180) and the National Key R&D Program of China (2017YFC 0507004).

References

Ahlrichs J.L., Serna C. & Serratosa J.M. (1975) Structural hydroxyls in sepiolite. *Clays and Clay Minerals*, **23**, 119–124.

Arundel A.V., Sterling E.M. & Biggin J.H. (1986) Indirect health-effects of relative-humidity in indoor environments. *Environmental Health Perspectives*, **65**, 351–361.

Chen S.G. & Yang R.T. (1996) Theoretical investigation of relationships between characteristic energy and pore size for adsorption in micropores. *Journal of Colloid and Interface Science*, **177**, 298–306.

Cho C.K. & You H.S. (2020) *Superabsorbent Resin Composite Having Improved Adsorption–Desorption Rate of Moisture in Air Useful as Humidity Control Material for Room and Package, and in Hygrometer System, Comprises Sepiolite*. South Korean Patent KR2020002114-A.

Gonzalez J.C., Molina-Sabio M. & Rodriguez-Reinoso F. (2001) Sepiolite-based adsorbents as humidity controller. *Applied Clay Science*, **20**, 111–118.

Gonzalez-Santamaria D.E., Lopez E. & Ruiz A. (2017) Adsorption of phenanthrene by stevensite and sepiolite. *Clay Minerals*, **52**, 341–350.

He R.T., Hu B.Y., Zhong H., Jin F.M., Fan J.J., Hu Y.H. & Jing Z.Z. (2019) Reduction of CO_2 with H_2S in a simulated deep-sea hydrothermal vent system. *Chemical Communications*, **55**, 1056–1059.

Inagaki S., Fukushima Y. & Doi H. (1990) Pore-size distribution and adsorption selectivity of sepiolite. *Clay Minerals*, **25**, 99–105.

Ishida E. H. (2002) Soil-ceramics (Earth), self-adjustment of humidity and temperature. P. 1019 in: *Encyclopedia of Smart Materials, Volume 1 and Volume 2*. Academic Press, New York, NY, USA.

Kai W., WeiMin G. & YunHua Q.I.N. (2011) The adsorption of volatile aldehydes and ketones in mainstream cigarette smoke by several adsorption materials. *Chinese Journal of Spectroscopy laboratory*, **28**, 1243–1248.

Lan H.R., Jing Z.Z. & Li J. (2017) Influence of pore dimensions of materials on humidity self-regulating performances. *Materials Letters*, **204**, 23–26.

Li J., Zhang W., Garbev K., Beuchle G. & Monteiro P.J.M. (2020) Influences of cross-linking and Al incorporation on the intrinsic mechanical properties of tobermorite. *Cement and Concrete Research*, **136**, 106170.

Liang X.F., Xu Y.M., Sun G.H., Wang L., Sun Y.B., Sun Y. & Qin X. (2011) Preparation and characterization of mercapto functionalized sepiolite and their application for sorption of lead and cadmium. *Chemical Engineering Journal*, **174**, 436–444.

Lyu L.Y., Zeng X., Yun J., Wei F. & Jin F.M. (2014) No catalyst addition and highly efficient dissociation of H_2O for the reduction of CO_2 to formic acid with Mn. *Environmental Science & Technology*, **48**, 6003–6009.

Miao J.J., Jing Z.Z., Pu L. & Zhang Y. (2018) Synthesis of a novel humidity self-regulating material from riverbed sediment for simulating cave dwellings performance. *Journal of Building Engineering*, **20**, 15–20

Ozcan A.S. & Gok O. (2012) Structural characterization of dodecyltrimethylammonium (DTMA) bromide modified sepiolite and its adsorption isotherm studies. *Journal of Molecular Structure*, **1007**, 36–44.

Sarıkaya Y., Önal M. & Pekdemir A. (2020) Thermal degradation kinetics of sepiolite. *Clay Minerals*, **55**, 96–100.

Shang J., Du Y.G. & Xu Z.L. (2002) Photocatalytic oxidation of heptane in the gas-phase over TiO_2. *Chemosphere*, **46**, 93–99.

Shen H. (2019) *Preparing Environmentally-Friendly Aqueous Antique Decorative Paint, Comprises e.g. Preparing Processed Sepiolite Powder, Mixing Processed Sepiolite Powder with Aqueous Solution of Potassium Permanganate-Reducing Potassium Permanganate*. Chinese Patent CN110591481-A.

Schreiner J., Goetz-Neunhoeffer F., Neubauer J. & Jansen D. (2020) Hydrothermal synthesis of 11 Å tobermorite – effect of adding metakaolin to the basic compound. *Applied Clay Science*, **185**, 105432.

Song Y., Qiao W. & Yoon S.H. (2007) Removal of formaldehyde at low concentration using various activated carbon fibers. *Journal of Applied Polymer Science*, **106**, 2151–2157.

Sun A., Delacaillerie J.B.D. & Fripiat J.J. (1995) A new microporous material – alminated sepiolite. *Microporous Materials*, **5**, 135–142.

Sun G., Jing Z., Cai L., Zhang Y., Zhao W. & Xu P. (2015) Hardening mechanism of low-temperature (100°C) solidification of clay brick waste containing NaOH. *Research on Chemical Intermediates*, **41**, 1373–1384.

Wu Y., Gong G.C. & Yu C.W. (2014) The hygroscopic properties of wood fiber, sepiolite and expanded perlite-based breathable wall for moderating the humidity environment. *Indoor and Built Environment*, **23**, 299–312.

Xu T.Z., Zheng H. & Zhang P.Y. (2018) Performance of an innovative VUV-PCO purifier with nanoporous TiO_2 film for simultaneous elimination of VOCs and by-product ozone in indoor air. *Building and Environment*, **142**, 379–387.

Yamaguchi K. (2012) *Humidity Control Decorative Board for Building Materials, Has Base Material Obtained by Forming Slurry Formed Using Sepiolite as Main Material, Sheet-Forming Fiber and Binder Resin, into Sheets*. Japanese Patent JP2012012900-A.

Zhang G.K. (2000) Development of sepiolite type filter tips of cigarette. *Journal of Wuhan University of Technology – Materials Science Edition*, **15**, 49–52.

Zhang Y., Jing Z.Z. & Fan X.W. (2013) Hydrothermal synthesis of humidity-regulating material from calcined loess. *Industrial & Engineering Chemistry Research*, **52**, 4779–4786.

https://doi.org/10.1180/clm.2021.1 Published online by Cambridge University Press